Pattern selection in rotating convection with experimental boundary conditions

Thomas Clune and Edgar Knobloch
Department of Physics, University of California, Berkeley, California 94720
(Received 14 October 1992)

Small-amplitude Boussinesq convection in a plane layer with rigid, conducting boundaries rotating uniformly about a vertical axis is studied. A horizontally unbounded layer is modeled by periodic boundary conditions and the effect of mean-flow suppression by distant sidewalls is considered. An exact linear stability calculation partitions parameter space into regions of stationary and oscillatory convective onset. In the stationary regime, the critical Taylor number and critical angle for the onset of the Küppers-Lortz instability are determined as a function of the Prandtl number σ. Of the two competing two-dimensional patterns in the oscillatory regime, traveling waves are the preferred planform for $0.442 < \sigma < 0.677$. For $\sigma < 0.442$ standing waves are preferred at onset for small rotation rates while traveling waves are preferred for larger rotation rates.

PACS number(s): 47.27.−i, 47.20.Ky

I. INTRODUCTION

Convection in a rotating plane layer heated from below is of interest for two fundamental reasons. First, for sufficiently small Prandtl numbers it can exhibit overstability, i.e., a Hopf bifurcation from the conduction state, that can be expected to lead to a variety of interesting dynamical phenomena, much like those studied extensively in binary fluid mixtures [1, 2]. In addition, however, the presence of rotation breaks reflection symmetry in vertical planes, thereby allowing new instabilities to occur as well. Of particular interest in this context is the so-called Küppers-Lortz instability discovered in 1969 [3]. This is an instability of a pattern of parallel rolls to a similar pattern but rotated through an angle α with respect to the original one. Since the new pattern that is established is itself unstable to the same instability, the instability inevitably leads to interesting time-dependent behavior. Küppers and Lortz [3] showed that for sufficiently fast rotation rates this instability sets in already at the threshold of the pattern-forming instability, suggesting that in this regime the conduction state loses stability directly to a spatiotemporally complex state.

The present paper is motivated by recent experiments [4,5] on this system. Specifically we are interested in providing precise and detailed predictions from the linear stability theory of the conduction state for experimentally measurable quantities such as the critical Rayleigh number, the wave number of the selected pattern, and the Hopf frequency (if the instability is oscillatory). The calculations are therefore carried out for the experimental boundary conditions and parameter values. The stability boundaries for the onset of both steady and oscillatory convection with no-slip and free-slip boundary conditions are found to become indistinguishable for sufficiently large rotation rates. This result, already well known for the onset of steady convection, can be supported by an asymptotic expansion in a small parameter (the Ekman or inverse Taylor number). In addition we present the results of weakly nonlinear calculations that enable us to compute accurately both the critical rotation rate beyond which rolls are Küppers-Lortz unstable as well as the angle with which the instability sets in. These quantities are a sensitive function of the Prandtl number, and here the results differ considerably from those with more idealized boundary conditions. The remainder of the paper is concerned with weakly nonlinear oscillatory convection. The calculations are restricted to two spatial dimensions so that the nonlinear problem concerns only traveling and standing waves. We determine the relative stability between these two patterns and show that either may be stable, depending on the system parameters. In this discussion we are careful to consider the impact of distant sidewalls in preventing the appearance of the mean flows that are associated with traveling patterns in unbounded systems. As in the Küppers-Lortz calculation we consider stability only with respect to perturbations of the same wave number as the basic pattern. Although this procedure excludes a large class of potentially important perturbations, prior experience suggests that the selected perturbations are the most dangerous. In addition this restriction enables us to rely on results obtained from equivariant bifurcation theory. This technique [6] allows us to classify the possible weakly nonlinear and spatially periodic states and establish their relative stability. In addition it identifies precisely the computations that have to be carried out on the partial differential equations in order to discriminate among the possible scenarios.

The paper is organized as follows. In the following section we summarize the relevant bifurcation theory results. In Sec. III we formulate the hydrodynamical equations and describe the technique we use to solve them. In Sec. IV we solve the linear stability problem for the conduction solution and identify regions in parameter space where oscillatory and steady-state convection takes place. In Sec. V we restrict the region of stable small-amplitude rolls by computing the location of the onset of

the Küppers-Lortz instability. In Sec. VI we determine the relative stability of standing and traveling waves in the oscillatory regime and thereby partition the parameter space even further. The results are discussed in Sec. VII.

II. PREDICTIONS FROM ABSTRACT THEORY

The Küppers-Lortz instability has a simple formulation. Since we are interested in the stability properties of a pattern of parallel rolls with respect to oblique roll-like disturbances we formulate the problem on a rhombic lattice whose angle α is to be specified. The lattice is defined by two wave vectors $\mathbf{k}_1$ and $\mathbf{k}_2$, each of magnitude k_c, selected from the circle of marginally stable modes together with their negatives, and satisfying $\mathbf{k}_1 \cdot \mathbf{k}_2 = k_c^2 \cos\alpha$. On such a lattice any weakly nonlinear pattern can be written in the form

$$w(\mathbf{x}, z, t) = \mathrm{Re}[\{z_1 e^{i\mathbf{k}_1 \cdot \mathbf{x}} + z_2 e^{i\mathbf{k}_2 \cdot \mathbf{x}}\} f_{k_c}(z) + \cdots]. \quad (1)$$

Here w is the vertical velocity, z_1 and z_2 are complex amplitudes specifying the amplitudes and phases of rolls with wave vectors $\mathbf{k}_1$ and $\mathbf{k}_2$, respectively, and $f_{k_c}(z)$ is the appropriate vertical eigenfunction. The form of the amplitude equations governing the evolution of these modes for slightly supercritical Rayleigh numbers is greatly restricted by the spatial symmetries of the system. These are the translations in the two directions together with the inversion symmetry $\mathbf{x} \to -\mathbf{x}$, as discussed by Knobloch and Silber [7]. The resulting equations truncated at third order are

$$\dot{z}_1 = (\mu + a|z_1|^2 + b_\alpha |z_2|^2) z_1, \quad (2a)$$

$$\dot{z}_2 = (\mu + a|z_2|^2 + b_{\overline{\alpha}} |z_1|^2) z_2, \quad (2b)$$

where $\mu \equiv (R - R_c)/R_c \ll 1$ and the coefficients a, b_α, and $b_{\overline{\alpha}}$ are real. Here R is the Rayleigh number and R_c its critical value at onset of convection. Note that the presence of rotation distinguishes between clockwise and counterclockwise directions; consequently the stability properties of rolls in the $\mathbf{k}_1$ direction with respect to perturbations in the $\mathbf{k}_2$ direction are not necessarily the same as those of rolls in the $\mathbf{k}_2$ direction with respect to perturbations in the $\mathbf{k}_1$ direction. Mathematically this fact manifests itself in the absence of the symmetry $z_1 \leftrightarrow z_2$ characteristic of nonrotating systems. As a result the coefficients b_α and $b_{\overline{\alpha}}$ are not forced to be identical; it is this fact that allows the Küppers-Lortz instability to take place. Note, however, that the coefficients a are identical. This fact is not forced by the symmetry of the rotating rhombic lattice but is a consequence of the SE(2) symmetry of the full unbounded problem. In particular the amplitudes of rolls in the $\mathbf{k}_1$ and $\mathbf{k}_2$ directions are the same.

Bifurcation theory tells us that for sufficiently small z_1 and z_2 Eqs. (2a) and (2b) capture all possible behavior of the system, provided $a \neq 0$, $b_\alpha - a \neq 0$, $b_{\overline{\alpha}} - a \neq 0$, and $b_\alpha b_{\overline{\alpha}} - a^2 \neq 0$. In terms of the real variables $z_j \equiv \rho_j e^{i\theta_j}$, $j = 1, 2$, Eqs. (2a) and (2b) become

$$\dot{\rho}_1 = (\mu + a\rho_1^2 + b_\alpha \rho_2^2)\rho_1, \quad (3a)$$

$$\dot{\rho}_2 = (\mu + a\rho_2^2 + b_{\overline{\alpha}} \rho_1^2)\rho_2, \quad (3b)$$

together with the two trivial equations $\dot{\theta}_1 = \dot{\theta}_2 = 0$. The spatial phases thus decouple and the system is described by a pair of real ordinary differential equations. The equations admit up to four fixed points for the dynamics:

Trivial	T	$\rho_1 = \rho_2 = 0$
Rolls	R	$\rho_1 = 0$ or $\rho_2 = 0$
Bimodal	B	$\rho_1 \neq \rho_2$, $\rho_1 \rho_2 \neq 0$.

In the following we refer to the two sets of rolls as R_1 ($\rho_2 = 0$) and R_2 ($\rho_1 = 0$). The branching equations and stability properties of the fixed points are summarized in Table I. Note in particular that the bimodal pattern exists only when the two sets of rolls are either both stable or both unstable, and that in the former case the pattern is necessarily unstable.

In Sec. V we shall see that with increasing rotation rate the coefficients b_α, $b_{\overline{\alpha}}$ begin to differ and that at large enough rotation rate $b_{\overline{\alpha}} - a$ passes through zero. As this happens the bimodal fixed point collides with R_1 and disappears forming a heteroclinic orbit connecting R_1 to R_2 (see Fig. 1). This is the mechanism by which rolls in one direction lose stability with respect to rolls at an angle α in the direction of rotation of the system. The angle α is chosen as that angle for which the bimodal pattern first disappears and is therefore the angle with which the Küppers-Lortz instability first manifests itself as the rotation rate is increased. We denote the critical Taylor number by τ_c and the corresponding angle by α_c. Note that in rotating convection the bimodal pattern never disappears by colliding with R_2; consequently $0 < \alpha_c < \pi/2$. In Sec. V we calculate the coefficients a, b_α, and $b_{\overline{\alpha}}$ from appropriate solvability conditions arising at third order in an amplitude expansion.

The competition between standing and traveling waves, hereafter denoted by SW and TW, respectively, is described by a very similar set of equations. In this case the initial instability is oscillatory with a Hopf frequency ω_c. The amplitude equations are [8]

TABLE I. The steady-state bifurcation on the rhombic lattice. A solution is stable if all of the signed quantities are negative. The bimodal pattern (B) exists only when both sets of rolls are stable or both are unstable.

Pattern	Branching equation	Stability
R_1	$\mu + a\rho^2 = 0$	$\mathrm{sgn}(a)$, $\mathrm{sgn}(b_{\overline{\alpha}} - a)$
R_2	$\mu + a\rho^2 = 0$	$\mathrm{sgn}(a)$, $\mathrm{sgn}(b_\alpha - a)$
B	$\mu(2a - b_{\overline{\alpha}} - b_\alpha) + (a^2 - b_\alpha b_{\overline{\alpha}})\rho^2 = 0$	$\mathrm{sgn}(a)$, $\mathrm{sgn}(b_\alpha b_{\overline{\alpha}} - a^2)$

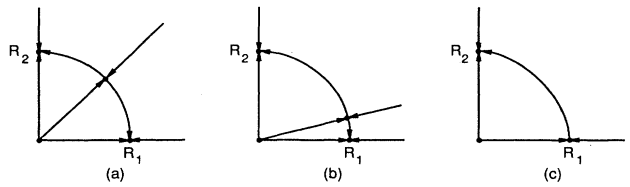

FIG. 1. Typical phase portraits showing the formation of the heteroclinic orbit responsible for the onset of the Küppers-Lortz instability. (a) The (ρ_1, ρ_2) plane for the nonrotating case ($b_\alpha = b_{\overline{\alpha}} < a < 0$). (b) The rotating case with no Küppers-Lortz instability ($b_\alpha < b_{\overline{\alpha}} < a < 0$), and (c) the rotating case with a Küppers-Lortz instability from R_1 to R_2 ($b_\alpha < a < b_{\overline{\alpha}}, a < 0$). The mixed mode no longer exists.

$$\dot{v} = [\mu + i\omega + b|w|^2 + a(|v|^2 + |w|^2) + \cdots]v, \quad (4a)$$

$$\dot{w} = [\mu - i\omega + \bar{b}|v|^2 + \bar{a}(|v|^2 + |w|^2) + \cdots]w, \quad (4b)$$

where (v, w) are complex amplitudes of left- and right-traveling waves, $\mu \equiv (R - R_c)/R_c$, $\omega - \omega_c = O(\mu)$, and a, b are now *complex* coefficients. In terms of (v, w) the vertical velocity of the fluid takes the form

$$w(x, z, t) = \mathrm{Re}[\{ve^{ik_c x} + \overline{w}e^{-ik_c x}\}f_{k_c}(z) + \cdots], \quad (5)$$

where $f_{k_c}(z)$ is again the vertical eigenfunction. Here R_c is the critical Rayleigh number at which the Hopf bifurcation first takes place and k_c is the wave number of the resulting waves. From Eqs. (4a) and (4b) it follows that stationary left TW are described by $(v, w) = (A_{TW}, 0)$, where

$$\mu + \mathrm{Re}(a)|A_{TW}|^2 + \cdots = 0, \quad (6)$$

while stationary SW are described by $(v, w) = (A_{\mathrm{SW}}, A_{\mathrm{SW}}e^{i\theta})/\sqrt{2}$, where

$$\mu + \mathrm{Re}(a + \tfrac{1}{2}b)|A_{\mathrm{SW}}|^2 + \cdots = 0. \quad (7)$$

Equations (4a) and (4b) also show that a stable solution will be present if and only if both TW and SW bifurcate supercritically, and that the stable one is the one with the larger mean-square amplitude [8]. In Table II we summarize the branching equations and the stability properties of each type of solution in terms of the coefficients $\mathrm{Re}(a)$ and $\mathrm{Re}(b)$. The resulting bifurcation diagrams are shown in Fig. 2.

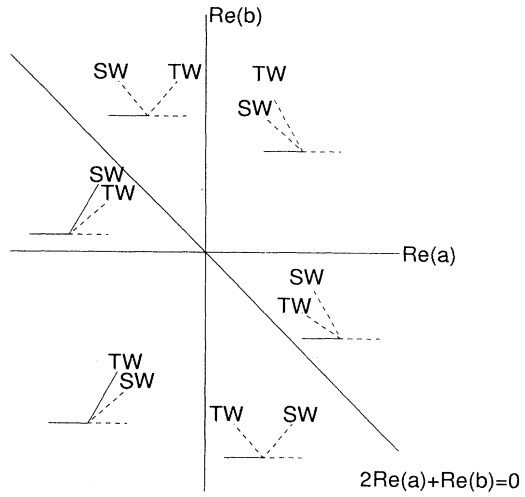

FIG. 2. Stability of traveling (TW) and standing (SW) waves in the $(\mathrm{Re}(a), \mathrm{Re}(b))$ plane. Solid (dashed) lines indicate stability (instability). Note that among the supercritical planforms the one with the largest amplitude is the stable one.

In Sec. VI these coefficients are computed for various values of the parameters. Two cases are considered, referred to as the unconstrained and constrained problems. The former is the formally unbounded problem with spatially periodic boundary conditions on all fields. This formulation allows the presence of constant mean flows that are associated with the TW. To model the effect of distant sidewalls in suppressing such mean flows we superpose in the constrained problem a constant pressure gradient just large enough to cancel the mean flow. Consequently while the pressure gradient remains periodic in space the pressure itself is no longer spatially periodic. This approach has been used before to study the effects of distant sidewalls on the oscillatory instability of rolls [9] and on TW convection in binary fluid mixtures [10], as well as the effects of distant ends on spiral vortices in the Taylor-Couette system [11]. Note that by suppressing the mean flow, the sidewalls or endwalls alter the values of the critical coefficients $\mathrm{Re}(a)$, $\mathrm{Re}(b)$ and hence alter the location in parameter space of stable TW and SW. In the following we deduce the coefficients $\mathrm{Re}(a)$ and $\mathrm{Re}(b)$ from the quantities r_2 specifying the direction of branching of both TW and SW. These are defined, as usual, by the expansion $R = R_c(1 + r_2|A|^2 + \cdots)$ where $|A|$ is the amplitude of each pattern. In view of the theory this calculation also determines the relative stability of the TW and SW (see Table II).

TABLE II. The Hopf bifurcation with O(2) symmetry. A solution is stable if the signed quantities are all negative.

Pattern	Branching equation	Stability
TW	$\mu + \mathrm{Re}(a)\|A\|^2 = 0$	$\mathrm{sgn}[\mathrm{Re}(a)]$, $\mathrm{sgn}[\mathrm{Re}(b)]$
SW	$\mu + [\mathrm{Re}(a) + \frac{1}{2}\mathrm{Re}(b)]\|A\|^2 = 0$	$\mathrm{sgn}[2\mathrm{Re}(a) + \mathrm{Re}(b)]$, $-\mathrm{sgn}[\mathrm{Re}(b)]$

III. FORMULATION AND METHOD OF SOLUTION

Boussinesq convection in a plane horizontal layer heated uniformly from below and rotating about the vertical with constant angular velocity $\Omega_{\rm phys}$ is described by the nondimensionalized equations

$$\partial_t \mathbf{u} + (\mathbf{u}\cdot\boldsymbol{\nabla})\mathbf{u} = -\boldsymbol{\nabla}\tilde{p} + \sigma\Theta\hat{\mathbf{z}} + \sigma\tau\mathbf{u}\times\hat{\mathbf{z}} + \sigma\nabla^2\mathbf{u}, \tag{8a}$$

$$\partial_t\Theta + (\mathbf{u}\cdot\boldsymbol{\nabla})\Theta = Rw + \nabla^2\Theta \tag{8b}$$

together with the incompressibility condition

$$\boldsymbol{\nabla}\cdot\mathbf{u} = 0 \tag{8c}$$

and appropriate boundary conditions at $z = \pm\frac{1}{2}$. Here $\mathbf{u} \equiv (u, v, w)$ is the velocity field in (x, y, z) coordinates, while $\tilde{p}$ and Θ denote the departures of the effective pressure and the temperature from their conduction profiles. Consequently the solution $\mathbf{u} = \Theta = \tilde{p} = 0$ corresponds to the pure conduction solution. The equations have been nondimensionalized with respect to the thermal diffusion time in the vertical. The system is specified by three dimensionless parameters: the Rayleigh number R, the Prandtl number σ, and the Taylor number τ^2 . The Taylor number is simply $(2\Omega)^2$, where $\Omega = \Omega_{\rm phys}h^2/\nu$ is the dimensionless angular velocity, h is the separation of the top and bottom plates, and ν is the kinematic viscosity. Note that results from the above formulation only apply to systems for which the Froude number $d\Omega^2_{\rm phys}/g$ is small so that centrifugal acceleration is small compared with gravity, and the buoyancy force continues to act in the z direction. Here d is the characteristic horizontal dimension of the system. This is the case in the recent experiments on large aspect ratio rotating convection in which the Froude number is typically at most 1% [5]. These experiments also motivate our choice of boundary conditions, no-slip, thermally conducting boundaries at top and bottom:

$$\mathbf{u} = \Theta = 0 \text{ at } z = \pm\tfrac{1}{2}. \tag{9}$$

As already explained in the preceding section we choose two types of boundary conditions in the horizontal. In the unconstrained case all fields are assumed to be spatially periodic functions in the $\mathbf{k}_{1,2}$ directions with spatial period $2\pi/k_c$, where k_c is the wave number of the mode that first becomes unstable as the Rayleigh number is increased. In the second, constrained, case we suppose that a mean pressure gradient $\xi \equiv \overline{\nabla\tilde{p}}$ is present and is determined by the requirement that no mean flow is present orthogonal to a sidewall. The difference between these two sets of boundary conditions manifests itself only for propagating patterns.

For computational convenience, we introduce poloidal and toroidal stream functions χ and ψ, respectively, such that

$$\mathbf{u} = \boldsymbol{\nabla}\times\boldsymbol{\nabla}\times\chi\hat{\mathbf{z}} + \boldsymbol{\nabla}\times\psi\hat{\mathbf{z}}. \tag{10}$$

Equations (8a) and (8b) can then be expressed in the abstract form

$$M\partial_t\phi = L\phi + N(\phi,\phi), \tag{11}$$

where M and L are given by

$$M = \begin{pmatrix} 1 & 0 & 0 \\ 0 & \nabla^2\nabla_H^2 & 0 \\ 0 & 0 & -\nabla_H^2 \end{pmatrix}, \tag{12}$$

$$L = \begin{pmatrix} \nabla^2 & -R\nabla_H^2 & 0 \\ -\sigma\nabla_H^2 & \sigma\nabla^4\nabla_H^2 & -\sigma\tau\nabla_H^2\partial_z \\ 0 & -\sigma\tau\nabla_H^2\partial_z & -\sigma\nabla^2\nabla_H^2 \end{pmatrix},$$

and

$$\phi = \begin{pmatrix} \Theta \\ \chi \\ \psi \end{pmatrix}. \tag{13}$$

We omit the explicit form of the nonlinear terms $N(\phi,\phi)$.

Care must be taken when translating the boundary conditions on $\mathbf{u}$ into boundary conditions on χ and ψ. The no-slip requirement

$$\partial^2_{xz}\chi + \partial_y\psi = \partial^2_{yz}\chi - \partial_x\psi = 0 \text{ at } z = \pm\tfrac{1}{2} \tag{14}$$

becomes $\partial_z\chi = 0$ at $z = \pm\frac{1}{2}$, but the introduction of the streamfunctions necessitates an additional boundary condition for χ and ψ on each surface. Gauge freedom allows us to specify $\chi = \psi = 0$ at $z = \frac{1}{2}$. It remains to specify the boundary conditions at $z = -\frac{1}{2}$. This is done in terms of (U, V), the components of the horizontal mean flow (if any). In view of the relations

$$U \equiv \int_{-1/2}^{1/2} u\,dz = \int_{-1/2}^{1/2} (\partial^2_{xz}\chi + \partial_y\psi)dz = (\partial_x\chi)|_{-1/2}^{+1/2} + \partial_y\int_{-1/2}^{1/2}\psi\,dz, \tag{15a}$$

$$V \equiv \int_{-1/2}^{1/2} v\,dz = \int_{-1/2}^{1/2} (\partial^2_{yz}\chi - \partial_x\psi)dz = (\partial_y\chi)|_{-1/2}^{+1/2} - \partial_x\int_{-1/2}^{1/2}\psi\,dz \tag{15b}$$

we may, without loss of generality, take the final two boundary conditions to be

$$\chi = -xU \text{ at } z = -\tfrac{1}{2} \text{ and } \int_{-1/2}^{1/2}\psi\,dz = -xV. \tag{16}$$

To determine the critical values R_c, k_c, and ω_c when the conduction solution loses stability to overstable convection ($\omega_c \neq 0$) or steady convection ($\omega_c = 0$), we look for solutions to the linearized equations of the form

$$\phi = e^{ikx}e^{(s_k + i\omega_k)t}\,f_k(z). \tag{17}$$

The condition $s_k = 0$ defines the neutral stability curve, and the critical Rayleigh number R_c is found by minimizing R over all k. This procedure yields k_c and hence ω_c. To find the coefficients of the nonlinear terms in the amplitude equations (2a) and (2b) and (4a) and (4b) we expand ϕ in powers of the (real) amplitude A of the motion,

$$\phi = A\phi^{(1)} + A^2\phi^{(2)} + \cdots, \tag{18}$$

normalizing $\phi^{(1)}$ such that

$$\langle\langle w^{(1)2}\rangle\rangle = 2, \tag{19}$$

where $\langle\langle\,\rangle\rangle$ denotes a time average over the period $2\pi/\omega_c$ of the oscillation, and a spatial average over a unit cell of the pattern. Here w is the vertical component of the velocity, and is given by $w = -\nabla_H^2\chi = k_c^2\chi$. The weakly nonlinear theory is most easily summarized in terms of the operator $\mathcal{L} \equiv M\partial_t - L$ representing the entire linear portion of the basic equations. Expanding R, ω, and $\mathcal{L}$ in powers of A,

$$R = R_c(1 + r_2A^2 + \cdots), \tag{20a}$$
$$\omega = \omega_c(1 + \omega_2A^2 + \cdots), \tag{20b}$$
$$\mathcal{L} = \mathcal{L}^{(0)} + \mathcal{L}^{(2)}A^2 + \cdots, \tag{20c}$$

and grouping like powers of A in Eq. (11) we obtain the hierarchy of equations

$$A^1: \quad \mathcal{L}^{(0)}\phi^{(1)} = 0, \tag{21a}$$
$$A^2: \quad \mathcal{L}^{(0)}\phi^{(2)} = N(\phi^{(1)}, \phi^{(1)}), \tag{21b}$$

$$A^3: \quad \mathcal{L}^{(0)}\phi^{(3)} = -\mathcal{L}^{(2)}\phi^{(1)} + N(\phi^{(1)}, \phi^{(2)}) + N(\phi^{(2)}, \phi^{(1)}). \tag{21c}$$

Equation (21a) is the linear stability problem and determines the various critical values k_c, R_c, and ω_c. The resulting eigenfunction $\phi^{(1)}$, normalized as in (19), is used to evaluate the nonlinear terms in (21b) and compute $\phi^{(2)}$. For TW traveling in the x direction terms of the form $(\chi, \psi) = (xf_1(z), xf_2(z))$ must be admitted in the solution at second order. These terms can be related to the mean gradients of $\tilde{p}$ by averaging the x and y components of the original fluid equations over the width $2\pi/k_c$ of a cell. Denoting such averages by overbars, one finds

$$\overline{\partial_t u^{(2)}} + \overline{(\mathbf{u}^{(1)}\cdot\nabla)u^{(1)}} = -\xi_x + \sigma\tau\overline{v^{(2)}} + \sigma\overline{\nabla^2 u^{(2)}}, \tag{22a}$$
$$\overline{\partial_t v^{(2)}} + \overline{(\mathbf{u}^{(1)}\cdot\nabla)v^{(1)}} = -\xi_y - \sigma\tau\overline{u^{(2)}} + \sigma\overline{\nabla^2 v^{(2)}}, \tag{22b}$$

where $(\xi_x, \xi_y) = (\overline{\partial_x\tilde{p}^{(2)}}, \overline{\partial_y\tilde{p}^{(2)}})$. The unconstrained case corresponds to $(\xi_x, \xi_y) = (0, 0)$ so that the TW is accompanied by mean flows in both the x and y directions. The experiments serve as a guide for choosing the boundary conditions for the constrained case. These are carried out in large aspect ratio cylindrical containers. In such containers the predicted TW travel in the *radial* direction. The container walls suppress the radial mean flow but the azimuthal mean flow remains unaffected. Thus the constrained problem is characterized by the requirements $U = 0$ and $\xi_y = 0$.

Finally, at third order, the existence of a solution requires the solvability condition

$$\langle\langle\phi^\dagger\cdot[-\mathcal{L}^{(2)}\phi^{(1)} + N(\phi^{(1)}, \phi^{(2)}) + N(\phi^{(2)}, \phi^{(1)})]\rangle\rangle = 0, \tag{23}$$

where $\phi^\dagger$ is any solution to the adjoint linear problem

$$\mathcal{L}^\dagger\phi^\dagger = 0. \tag{24}$$

Here

$$\mathcal{L}^\dagger = -M\partial_t - L^\star, \tag{25}$$

where $\star$ denotes the transpose of L followed by changing the sign of z. The adjoint problem is to be solved subject to appropriate boundary conditions. These are the same as those for ϕ but applied at $z = \mp\frac{1}{2}$ instead of $z = \pm\frac{1}{2}$. Since the layer is symmetric about the midplane $z = 0$ it is possible, therefore, to find the adjoint eigenfunctions in terms of the solutions $\phi^{(1)}$ by suitable reflections in $z = 0$, scalings and time reversals. Consequently the solution of the adjoint problem requires no further computation. Substituting for $\mathcal{L}^{(2)}$ into Eq. (23), we obtain two equations (real and imaginary parts) determining r_2 and ω_2.

With the boundary conditions (9) the above calculations must be carried out numerically. The linear stability problem is solved as in [12]; the remainder of the calculations were done using the package PATTERN SELECTION written in MATHEMATICA, the details of which will be presented elsewhere [13].

IV. LINEAR STABILITY RESULTS

The linear stability problem with no-slip boundary conditions has been considered before by Chandrasekhar [14], Clever and Busse [15], and most recently by Ardron, Lucas, and Stein [16]. Chandrasekhar's results were obtained using mostly variational techniques, while Clever and Busse employed a Galerkin expansion. The technique employed by Ardron, Lucas, and Stein relies on the resummation of a series representation of the solution and is in principle exact. This paper focuses, however, on rotating binary mixtures and does not present detailed results for pure fluids. In the following we obtain exact solutions of the linear stability problem following the work of Knobloch and Moore [12]. We employ the parameters from the recent experiments on water [4, 5], compressed CO_2 gas [17], and liquid ^{4}He above the λ point [18, 19]. These systems are primarily distinguished by their Prandtl numbers, these being $\sigma = 6.8$, 0.80, and 0.49, respectively. In addition we examine $\sigma = 0.40$, 0.30, and 0.025, the latter being of interest to earlier experiments on mercury [20]. This section is divided into three parts. In the first we describe the construction of the solution. The second is devoted to the large rotation rate limit and demonstrates that in this limit the linear stability results with no-slip boundary conditions approach asymptotically those for stress-free boundary conditions. The results, presented in Sec. IV C, have been checked using a variant of the numerical code used in Ref. [12] provided by Dr. D. R. Moore.

A. Construction of the solution

The stability of the conduction state is governed by Eq. (21a). Translational symmetry allows us to seek so-

lutions of this system in the form (17), with $f_k(z) \equiv (f_k^\Theta, f_k^\chi, f_k^\psi)$. Because of rotational symmetry f_k, s_k, and ω_k can only depend on $k = |\mathbf{k}|$. Since the linearized equations are homogeneous in z, the two-point boundary problem in the vertical specifying f_k can be solved exactly. This problem is of eighth order but in view of the reflection symmetry about $z = 0$ the eight eigenvalues take the form $\pm\lambda_j$, $j = 0, ..., 3$. The general solution thus takes the form

$$f_k^\Theta(z) = \sum_{j=0}^{3} A_j \frac{\cosh \lambda_j z}{\cosh \lambda_j/2}, \tag{26a}$$

$$f_k^\chi(z) = \sum_{j=0}^{3} A_j \frac{k^2 + i\omega - \lambda_j^2}{Rk^2} \frac{\cosh \lambda_j z}{\cosh \lambda_j/2}, \tag{26b}$$

$$f_k^\psi(z) = \sum_{j=0}^{3} A_j \frac{\tau\sigma\lambda_j(\lambda_j^2 - k^2 - i\omega)}{Rk^2(\sigma(\lambda_j^2 - k^2) - i\omega)} \frac{\sinh \lambda_j z}{\cosh \lambda_j/2}. \tag{26c}$$

Substituting these expressions into the boundary conditions, we find that the condition for the existence of a nontrivial solution takes the form

$$\det \begin{pmatrix} 1 & 1 & 1 & 1 \\ (\lambda_0^2 - k^2 - i\omega) & (\lambda_1^2 - k^2 - i\omega) & (\lambda_2^2 - k^2 - i\omega) & (\lambda_3^2 - k^2 - i\omega) \\ \gamma_0(\lambda_0^2 - k^2 - i\omega) & \gamma_1(\lambda_1^2 - k^2 - i\omega) & \gamma_2(\lambda_2^2 - k^2 - i\omega) & \gamma_3(\lambda_3^2 - k^2 - i\omega) \\ \gamma_0 \frac{(\lambda_0^2 - k^2 - i\omega)}{\sigma(\lambda_0^2 - k^2) - i\omega} & \gamma_1 \frac{(\lambda_1^2 - k^2 - i\omega)}{\sigma(\lambda_1^2 - k^2) - i\omega} & \gamma_2 \frac{(\lambda_2^2 - k^2 - i\omega)}{\sigma(\lambda_2^2 - k^2) - i\omega} & \gamma_3 \frac{(\lambda_3^2 - k^2 - i\omega)}{\sigma(\lambda_3^2 - k^2) - i\omega} \end{pmatrix} = 0, \tag{27}$$

where

$$\gamma_j \equiv \lambda_j \tanh \lambda_j/2. \tag{28}$$

These results reduce to those for steady convection when $\omega = 0$; they can also be used to compute the growth rates for supercritical values of R by replacing $i\omega$ by $s + i\omega$, where s is the growth rate.

The above condition thus determines $R(k)$ for steady convection, as well as $R(k)$ and $\omega(k)$ for oscillatory convection. Minimization of $R(k)$ with respect to k determines R_c and ω_c, as well as k_c. If the overstable critical Rayleigh number R_c^{Hopf} is less than the stationary Rayleigh number R_c^{SS} convection is overstable; otherwise it is stationary.

B. Large-τ limit

In this section, we extend earlier work of Niiler and Bisshopp [21] to show that, in the limit of large Taylor numbers, the linear stability properties of the conduction solution for stress-free and rigid boundaries are asymptotically indistinguishable. In particular, we generalize the previous analysis to include the possibility of overstable convection and show that the effects of the no-slip boundary conditions are compressed into thinner and thinner boundary layers as the Taylor number increases. For stress-free boundaries, one finds that the minimum Taylor number for overstable convection diverges as the Prandtl number approaches a critical Prandtl number $\sigma^\star$, above which there can be no oscillatory convection. The following arguments show that one expects the same behavior for rigid boundaries, and in particular that the critical Prandtl number $\sigma^\star$ remains unchanged.

The characteristic polynomial $P(\lambda)$ determining the eigenvalues λ describing the vertical structure follows from Eq. (21a). With the scaling

$$R = \tilde{r}\tau^{4/3}, \tag{29a}$$

$$k = \tilde{k}\tau^{1/3}, \tag{29b}$$

$$\omega = \tilde{\omega}\tau^{2/3} \tag{29c}$$

the polynomial takes the form

$$P(\lambda) = \sigma^2\lambda^8 + B_3\lambda^6 + B_2\lambda^4 + B_1\lambda^2 + B_0, \tag{30}$$

where

$$B_0 = \tau^{8/3}\tilde{k}^2(\sigma\tilde{k}^2 + i\tilde{\omega})[\sigma\tilde{k}^4 + i\tilde{\omega}\tilde{k}^2(1+\sigma) - \tilde{\omega}^2 - \sigma\tilde{r}], \tag{31a}$$

$$B_1 = -\tau^2[\, 4\sigma^2\tilde{k}^6 + 3i\tilde{\omega}\tilde{k}^4\sigma(2+\sigma) - 2\tilde{k}^2\tilde{\omega}^2(1+2\sigma) - i\tilde{\omega}^3 - \sigma^2\tilde{k}^2\tilde{r}] \tag{31b}$$

$$-\tau^{8/3}\sigma^2(\tilde{k}^2 + i\tilde{\omega}), \tag{31c}$$

$$B_2 = -\tau^{4/3}[\, -6\sigma^2\tilde{k}^4 - 3i\tilde{\omega}\tilde{k}^2\sigma(2+\sigma) + \tilde{\omega}^2(1+2\sigma)] + \tau^2\sigma^2, \tag{31d}$$

$$B_3 = -\tau^{2/3}\sigma[i\tilde{\omega}(2+\sigma) + 4\sigma\tilde{k}^2]. \tag{31e}$$

The roots of this polynomial have the asymptotic form

$$\lambda_0^2 = (\tilde{k}^2 + i\tilde{\omega})\tau^{2/3}[1 + O(\tau^{-2/3})], \tag{32a}$$

$$\lambda_1^2 = \frac{\tilde{k}^2(\sigma\tilde{k}^2 + i\tilde{\omega})[\sigma\tilde{k}^4 + i\tilde{\omega}\tilde{k}^2(1+\sigma) - \tilde{\omega}^2 - \sigma\tilde{r}]}{\sigma^2(\tilde{k}^2 + i\tilde{\omega})} \times[1 + O(\tau^{-2/3})], \tag{32b}$$

$$\lambda_2^2 = i\tau[1 + O(\tau^{-1/3})], \tag{32c}$$

$$\lambda_3^2 = -i\tau[1 + O(\tau^{-1/3})]. \tag{32d}$$

Substituting these expressions into (27) we obtain, to leading order in τ, the condition

$$\det\begin{pmatrix} 1 & 1 & 1 & 1 \\ O(\tau^0) & -(\tilde{k}^2+i\tilde{\omega})\tau^{2/3}+O(\tau^0) & i\tau+O(\tau^{2/3}) & -i\tau+O(\tau^{2/3}) \\ O(\tau^{1/3}) & -\gamma_1[(\tilde{k}^2+i\tilde{\omega})\tau^{2/3}+O(\tau^0)] & (i\tau)^{3/2}+O(\tau^{7/6}) & (-i\tau)^{3/2}+O(\tau^{7/6}) \\ O(\tau^{-1/3}) & \gamma_1[\frac{\tilde{k}^2+i\tilde{\omega}}{\sigma\tilde{k}^2+i\tilde{\omega}}+O(\tau^{-2/3})] & \frac{(i\tau)^{1/2}}{\sigma}+O(\tau^{1/6}) & \frac{(-i\tau)^{1/2}}{\sigma}+O(\tau^{1/6}) \end{pmatrix}=0. \tag{33}$$

As before, this condition determines $\tilde{r}$ and $\tilde{\omega}$. For large τ these quantities satisfy

$$\gamma_1=-\frac{\sqrt{2}(\sigma\tilde{k}^2+i\tilde{\omega})}{\sigma}\tau^{1/6}+O(\tau^{-1/6}), \tag{34}$$

with γ_1 defined as in (28). Since γ_1 diverges while λ_1 remains finite as τ increases, λ_1 must be near some multiple of $i\pi$. The most unstable mode corresponds to $\lambda_1^2\equiv-\pi^2$. Thus

$$\lambda_1=i\pi\left(1-\frac{\sigma\sqrt{2}}{\sigma\tilde{k}^2+i\tilde{\omega}}\tau^{-1/6}\right)+O(\tau^{-1/3}). \tag{35}$$

The corresponding results for steady convection follow from those given above on setting $\tilde{\omega}=0$.

Consequently the limiting form of this eigenvalue corresponds to the sole eigenvalue, $i\pi$, present for stress-free boundary conditions. Moreover, the contributions of the remaining eigenvalues vanish asymptotically everywhere except in exponentially thin boundary layers near $z=\pm\frac{1}{2}$. As a result in the limit of large rotation rates the solutions of the linear stability problem with stress-free and no-slip boundary conditions become identical. In particular R_c, k_c, and ω_c are the same for both problems. Note, however, that the approach to this asymptotic regime is very slow. Since the error term in Eq. (35) is $O(\tau^{-1/6})$, the asymptotic regime is only reached when $\tau=O(10^6)$ or larger. Since all of the nonlinear calculations depend solely on the vertical structure of the linear solution, we can also conclude that pattern selection is independent of boundary conditions for large τ. In particular it follows that traveling waves will be the selected planform in this regime regardless of the boundary conditions [22]. The above conclusions hold for $\sigma=O(1)$ or larger, but will be modified in the limit $\sigma\to0$.

From the stress-free case, we know that [14]

$$\tilde{r}^{\rm Hopf}=\tfrac{3}{2}(1+\sigma)\left(\frac{2\pi\sigma}{1+\sigma}\right)^{4/3}, \tag{36a}$$

$$\tilde{k}^{\rm Hopf}=\left(\frac{\pi^2\sigma^2}{2(1+\sigma)^2}\right)^{1/6}, \tag{36b}$$

$$\tilde{\omega}^2=\tfrac{1}{4}(2-3\sigma^2)\left(\frac{2\pi\sigma}{1+\sigma}\right)^{4/3} \tag{36c}$$

for oscillatory convection, while

$$\tilde{r}^{\rm SS}=3\left(\frac{\pi^2}{2}\right)^{2/3}, \tag{37a}$$

$$\tilde{k}^{\rm SS}=\left(\frac{\pi^2}{2}\right)^{1/6} \tag{37b}$$

for steady convection. The requirement that $\tilde{r}^{\rm Hopf}=\tilde{r}^{\rm SS}$ determines the critical value $\sigma^\star$ of the Prandtl number separating oscillatory from steady convection in the limit of large τ:

$$8\sigma^4=\sigma+1. \tag{38}$$

Thus $\sigma^\star=0.676\,605\ldots$ as obtained already by Chandrasekhar [14]. The foregoing analysis shows that the above value of $\sigma^\star$ applies to no-slip boundary conditions as well. This result differs from the conclusion of Ref. [16].

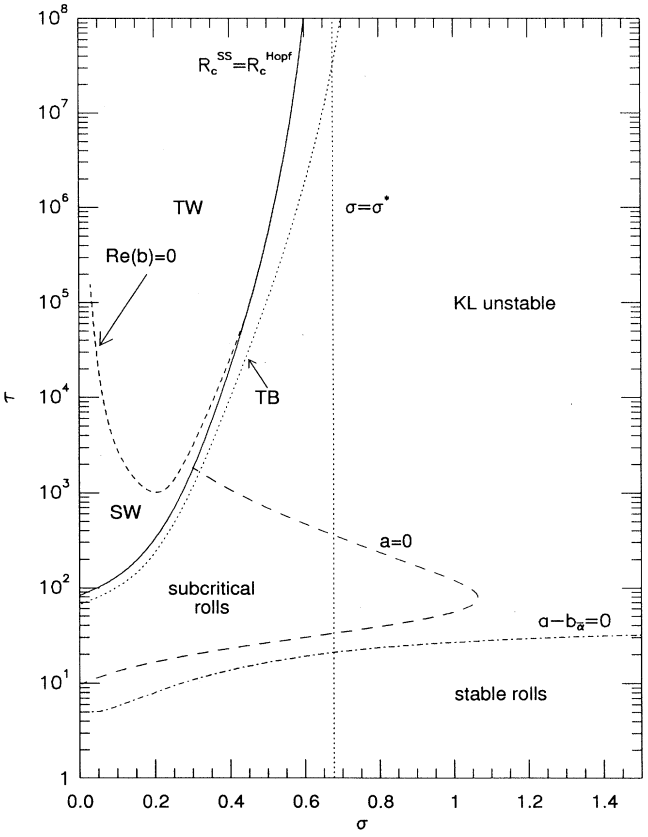

FIG. 3. The (σ,τ) plane showing the curve of the codimension-2 bifurcations (——) separating overstable from steady convection. The short-dashed line (- - -) divides the former into regions of preferred traveling waves and preferred standing waves. The long-dashed line (– – –) shows the curve $r_2^R=0$ for steady rolls, while the dashed-dotted line (-·-·-) indicates the onset of the Küppers-Lortz instability. No overstable convection is possible for $\sigma>\sigma^\star=0.677$ as indicated by the vertical dotted line (···). The remaining dotted line indicates the Takens-Bogdanov curve defined by $\omega_c=0$.

C. Results

The solid line in the (σ,τ) plane shown in Fig. 3 separates the regions of overstable and steady convection. The line is defined by $R_c^{\rm Hopf}(k_c^{\rm Hopf}) = R_c^{\rm SS}(k_c^{\rm SS})$. Since this point is a codimension-2 point we denote it in the following by $R_{\rm CT}$ and its locus in the (σ,τ) plane by $\tau_{\rm CT}(\sigma)$ [23]. The asymptote $\sigma = \sigma^\star$ is indicated. The general form of the CT curve resembles that for stress-free boundaries [22], except that it is, as expected, shifted to substantially higher values of τ. Figure 3 illustrates well the very slow approach to $\sigma^\star$ with increasing τ noted above. For example, at $\sigma = 0.49$ $\tau_{\rm CT}$ is already 3.44×10^5, well beyond the highest Taylor number used in the experiment of Ref. [19]. In Figs. 4 and 5 we look at the linear stability results in more detail. Figure 4 shows the τ dependence of the linear stability results over a substantial range of values of τ. In view of the strong dependence of the results on τ we present in Fig. 4 the critical Rayleigh number, wave number, and frequency scaled as in Eq. (29). Thus Fig. 4(a) shows $\tilde{r}_c$ as a function of τ for $\sigma = 0.025$, 0.30, 0.40, and 0.49. The solid lines indicate the onset of overstability; the dashed line is the critical Rayleigh number for steady convection and is independent of σ. The remaining panels show the critical wave numbers $\tilde{k}_c$ and the corresponding frequencies $\tilde{\omega}_c$; the final panel shows the phase velocity ω_c/k_c and the group velocity $\partial\omega/\partial k$ evaluated at $k = k_c$. Note that the group velocity is typically in the direction opposite to the phase velocity. Figure 5 describes the σ dependence of these quantities for $\tau = 200$, 1000, 4000, and 10 000. Panel (a) shows that the critical Rayleigh numbers for oscillatory convection increase with σ; at the CT point oscillatory convection is superseded by steady convection

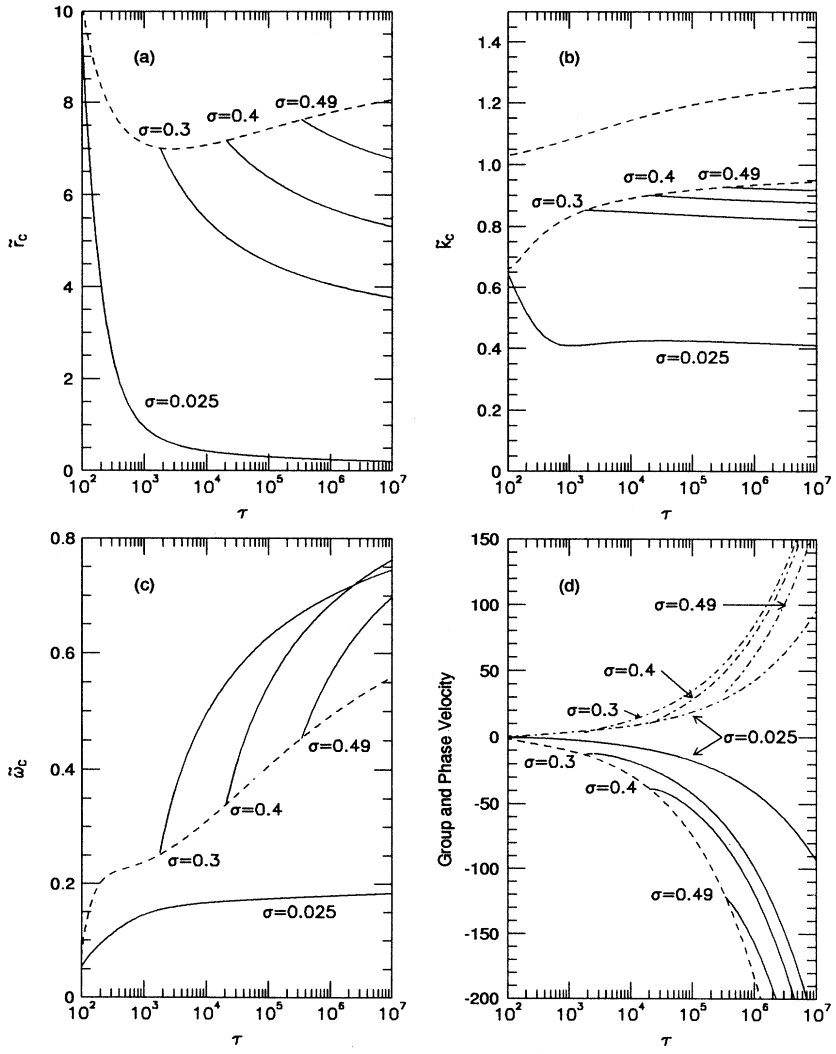

FIG. 4. Linear stability results as a function of τ for several values of σ. (a) The scaled critical Rayleigh number $\tilde{r}_c$. The dashed line indicates $\tilde{r}_{\rm CT}$. (b) The scaled critical wave number $\tilde{k}_c$. The dashed lines indicate $\tilde{k}_{\rm CT}^{\rm Hopf}$ and $\tilde{k}_{\rm CT}^{\rm SS}$. (c) The scaled Hopf frequency $\tilde{\omega}_c$. The dashed line indicates $\tilde{\omega}_{\rm CT}$. (d) The group velocity (solid lines) and the phase velocity (dashed-dotted lines). The dashed line indicates the group velocity along the CT curve.

with R_c independent of the Prandtl number. Panel (b) shows the corresponding critical wave numbers, and indicates the origin of the wave-number jumps that occur in the transition from overstable to steady convection. The σ or equivalently the τ dependence of the wave-number jump is shown on a logarithmic scale in Fig. 6 as is the corresponding jump in frequency, from $\omega_{\rm CT}$ at the CT point to zero. Note that the Hopf frequency reaches a maximum as a function of σ before decreasing to its value $\omega_{\rm CT}$ at the codimension-2 point [Fig. 5(c)].

For comparison with a similar study of binary fluid mixtures [12] we show in Fig. 7 the quantity $\Delta R \equiv R_{\rm CT} - R_{\rm TB}$ as a function of σ. Here $(R_{\rm TB}, \tau_{\rm TB}(\sigma))$ is the Takens-Bogdanov point defined to be the point at which the Hopf frequency vanishes, i.e., $\omega_c \equiv \omega(k_c^{\rm Hopf}) = 0$. Note that in contrast to the binary fluid mixtures ΔR is relatively large. Consequently the dynamics associated with the Takens-Bogdanov point are much less likely to be of interest for rotating convection. This conclusion comes as no surprise, since unlike binary mixtures, in rotating convection ΔR does not vanish even with stress-free boundaries [22]. The Takens-Bogdanov point is shown in Fig. 3 as the dotted line to the right of the CT curve.

For many purposes it is also important to understand the (slow) response of the system when subjected to large scale modulation such as might arise from distant sidewalls. Such a response is described by evolution equations in slow spatial and temporal variables. For such equations one needs to know the curvature of the curve $R(k)$ at $k = k_c$, and the derivatives of the frequency with respect to both wave number and Rayleigh number [24]. In Fig. 8 we therefore show the τ dependence of the quantities $\xi_0^2 \equiv \frac{1}{2R_c}\frac{\partial^2 R}{\partial k^2}|_{k_c}$, $c_1 \equiv \frac{1}{2}\tau_0\xi_0^{-2}\frac{\partial^2\omega}{\partial k^2}|_{k_c}$, $\tau_0^{-1} \equiv R_c\frac{\partial s}{\partial R}|_{R_c}$, and $c_0 \equiv R_c\tau_0\frac{\partial\omega}{\partial R}|_{R_c}$ evaluated for oscil-

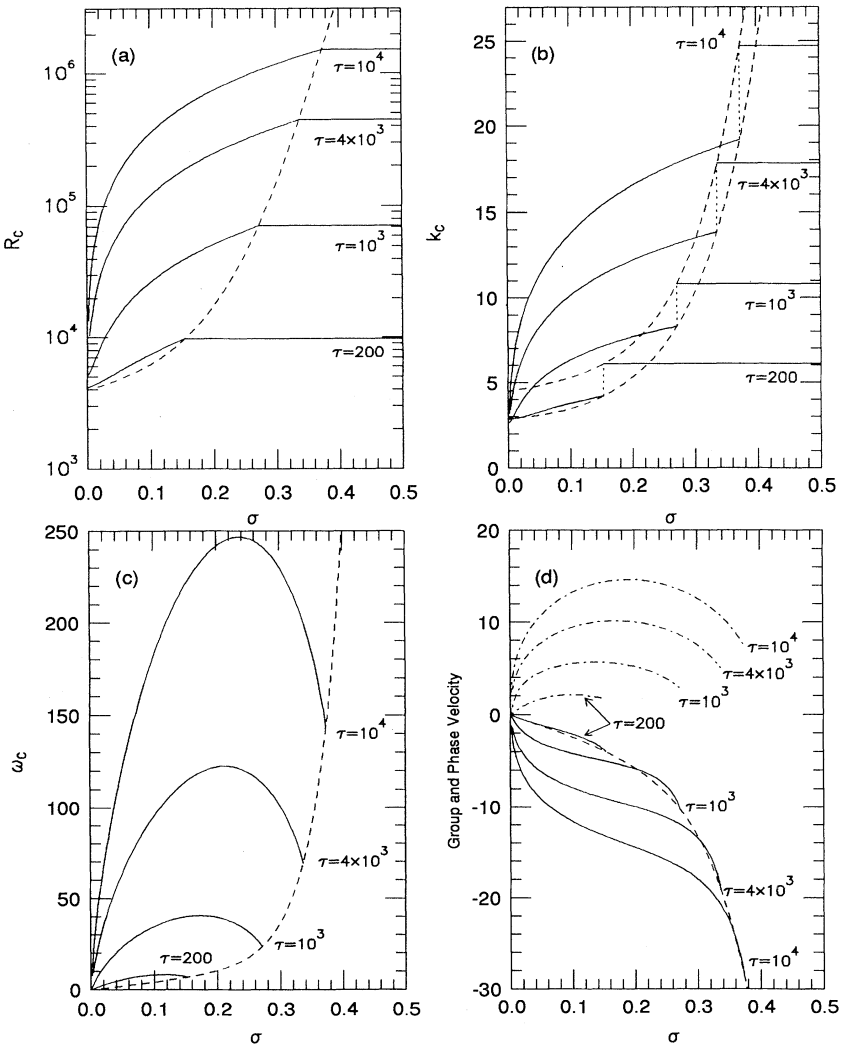

FIG. 5. Same as Fig. 4 but showing unscaled quantities as a function of σ for several values of τ. In (b) the dotted lines indicate the jump in k_c across the CT curve.

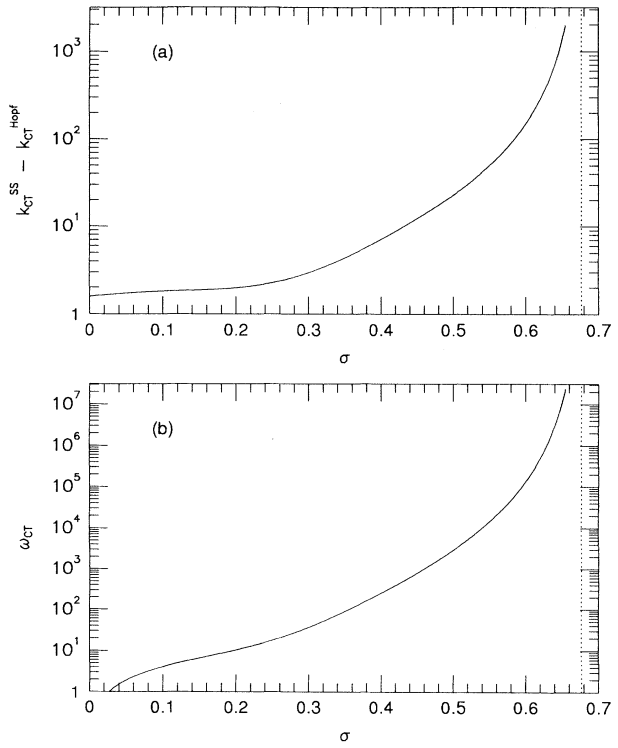

FIG. 6. (a) The jump in k_c across the CT curve as a function of σ. (b) The corresponding jump in ω_c. The dotted line indicates $\sigma = \sigma^\star$.

latory convection, while Fig. 9 shows the corresponding σ dependence. Finally Fig. 10 shows τ_0^{-1} and ξ_0^2 for steady convection as functions of τ.

V. THE KÜPPERS-LORTZ INSTABILITY

The onset of the Küppers-Lortz instability with no-slip boundary conditions was studied for general Prandtl numbers by Küppers [25] but the results are not sufficiently detailed for today's experiments. We have therefore employed the method summarized in Sec. III to re-examine the stability of small-amplitude rolls in the stationary regime. As discussed in Sec. II the stability of rolls with respect to perturbations on a rhombic lattice depends on the nonlinear coefficients in the amplitude equations (2a) and (2b). These coefficients are in turn directly related to the r_2's of the competing planforms. For the roll planform,

$$\phi^{(1)} = A\mathrm{Re}[e^{i\mathbf{k}_1\cdot\mathbf{x}} f_{k_c}(z)], \tag{39}$$

we find $a = -r_2^R$, while for the bimodal planform,

$$\phi^{(1)} = A\mathrm{Re}[\{\cos\beta\, e^{i\mathbf{k}_1\cdot\mathbf{x}} + \sin\beta\, e^{i\mathbf{k}_2\cdot\mathbf{x}}\} f_{k_c}(z)], \tag{40}$$

we find

$$r_2^B = -a\cos^2\beta - b_\alpha \sin^2\beta = -a\sin^2\beta - b_{\overline{\alpha}}\cos^2\beta. \tag{41}$$

These relations determine a, b_α, and $b_{\overline{\alpha}}$ in terms of r_2^R, r_2^B, and the arbitrary angle $\beta \in [0,\pi]$. Figure 3 shows the line $r_2^R = 0$. This line intersects the CT line at a codimension-3 point with coordinates $\sigma = 0.30$, $\tau = 1833$, and $R = 1.6 \times 10^5$. The bifurcation to steady rolls is generally supercritical ($r_2^R > 0$) except at small Prandtl numbers where it is subcritical ($r_2^R < 0$). The occurrence of subcritical steady convection is well known for free boundaries and agrees with the calculation of Ref. [15] with rigid boundaries. Note, however, that the region of subcritical steady convection lies entirely in the Küppers-Lortz unstable region (see below) so that subcritical steady convection is not expected to be observable.

As already mentioned, the rolls R_1 lose stability with increasing τ to R_2 when $b_{\overline{\alpha}} = a$, i.e., when $\beta = 0$ or equivalently when $r_2^B = r_2^R$. To locate the onset of this instability we vary τ and solve

$$\min_{\alpha\in[0,\pi]}[a(\sigma,\tau) - b_{\overline{\alpha}}(\sigma,\tau)] = 0. \tag{42}$$

The solution τ_c and the corresponding angle α_c are shown as a function of the Prandtl number in Fig. 11, as are the corresponding Rayleigh number and wave number. Some particular examples are listed in Table III. The location of the Küppers-Lortz instability in the (σ,τ) plane is shown in Fig. 3 as the dashed-dotted line.

It is worth noting that the corresponding results for

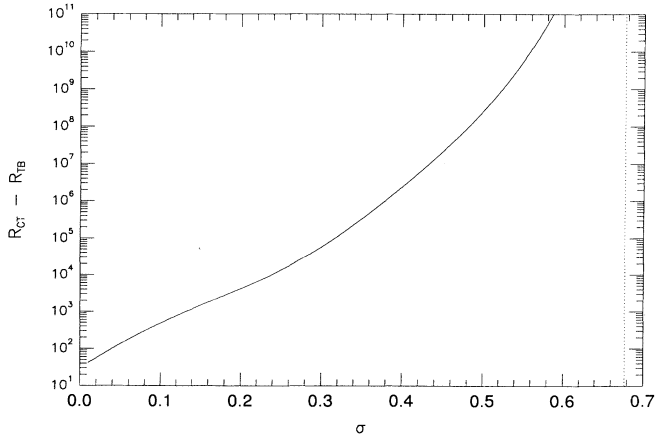

FIG. 7. Difference in the Rayleigh numbers between the CT and TB curves. The dotted line indicates $\sigma = \sigma^\star$.

TABLE III. The onset of the Küppers-Lortz instability as a function of the Prandtl number.

σ	τ_c	α_c	k_c	R_c
0.025	5.01	11.6	3.13	1720
0.3	10.9	23.0	3.17	1766
0.4	13.8	26.7	3.20	1800
0.49	16.4	29.6	3.23	1836
0.6	19.2	32.9	3.27	1882
0.8	23.6	38.4	3.34	1966
6.8	46.2	59.1	3.78	2577
∞	54.8	59.7	3.95	2868

stress-free boundaries are qualitatively different. As observed first by Swift [26], with stress-free boundaries the rolls R_1 are *always* Küppers-Lortz unstable against rolls inclined at a sufficiently small angle α with respect to them. In Fig. 12(a) we show $a - b_{\overline{\alpha}}$ for $\sigma = 100$, as a function of α for τ both below and above the corresponding $\tau_c = 46$. Observe that for $\tau < \tau_c$ this quantity is indeed positive for most values of α, although it diverges to $\mp\infty$ for α near zero and π, respectively. This fact was apparently missed by Küppers and Lortz [3] because of the assumption of infinite Prandtl number: the singularities at small α and near $\alpha = \pi$ disappear in this limit [Fig. 12(b)]. For finite Prandtl numbers no-slip boundary conditions are required to stabilize these small angle instabilities. Only in this case is the instability as described by Küppers and Lortz in their original paper [3].

VI. STANDING AND TRAVELING WAVES

The region of parameter space in which the onset of convection is overstable can likewise be divided into regions of distinct nonlinear behavior. In two dimensions this behavior is described by Eqs. (4a) and (4b). The real parts of the coefficients in these equations are related to the r_2's by

$$r_2^{\mathrm{TW}} = -\mathrm{Re}(a), \tag{43a}$$

$$r_2^{\mathrm{SW}} = -\mathrm{Re}(a) - \tfrac{1}{2}\mathrm{Re}(b). \tag{43b}$$

The traveling waves bifurcate supercritically if $r_2^{\mathrm{TW}} > 0$, the standing waves if $r_2^{\mathrm{SW}} > 0$.

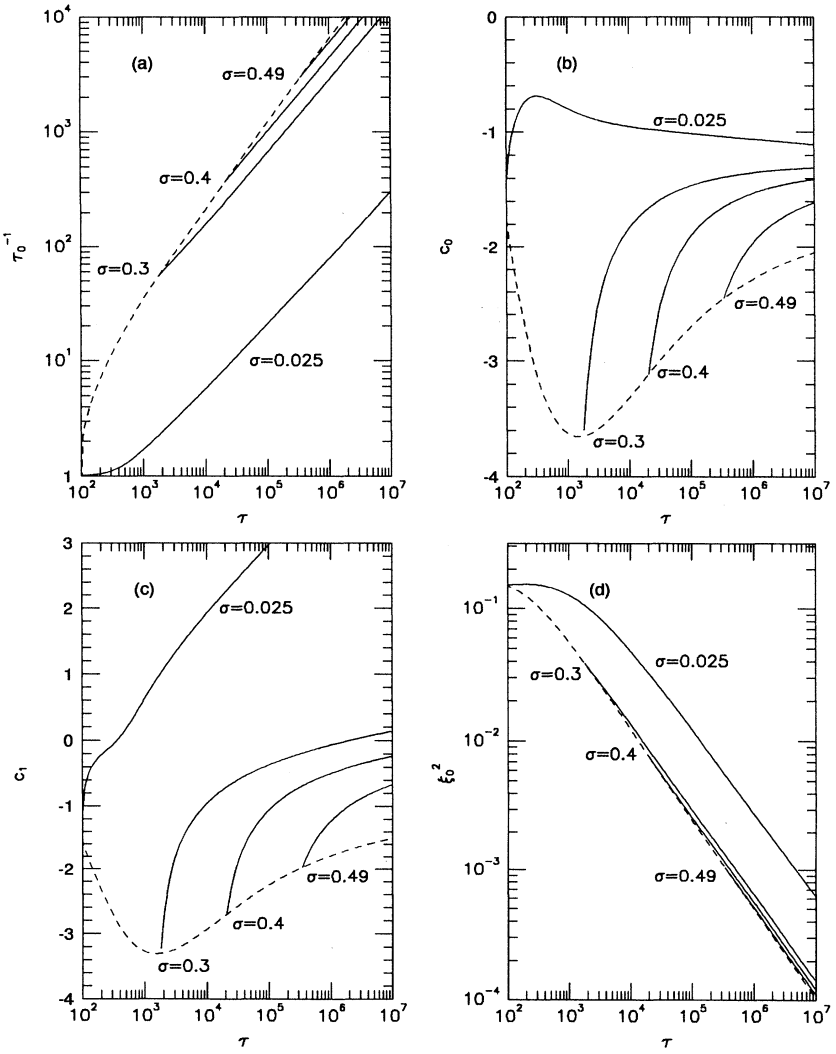

FIG. 8. The coefficients (a) τ_0^{-1}, (b) c_0, (c) c_1, (d) ξ_0^2 as a function of τ for several values of σ. The dashed lines indicate the corresponding values along the CT curve.

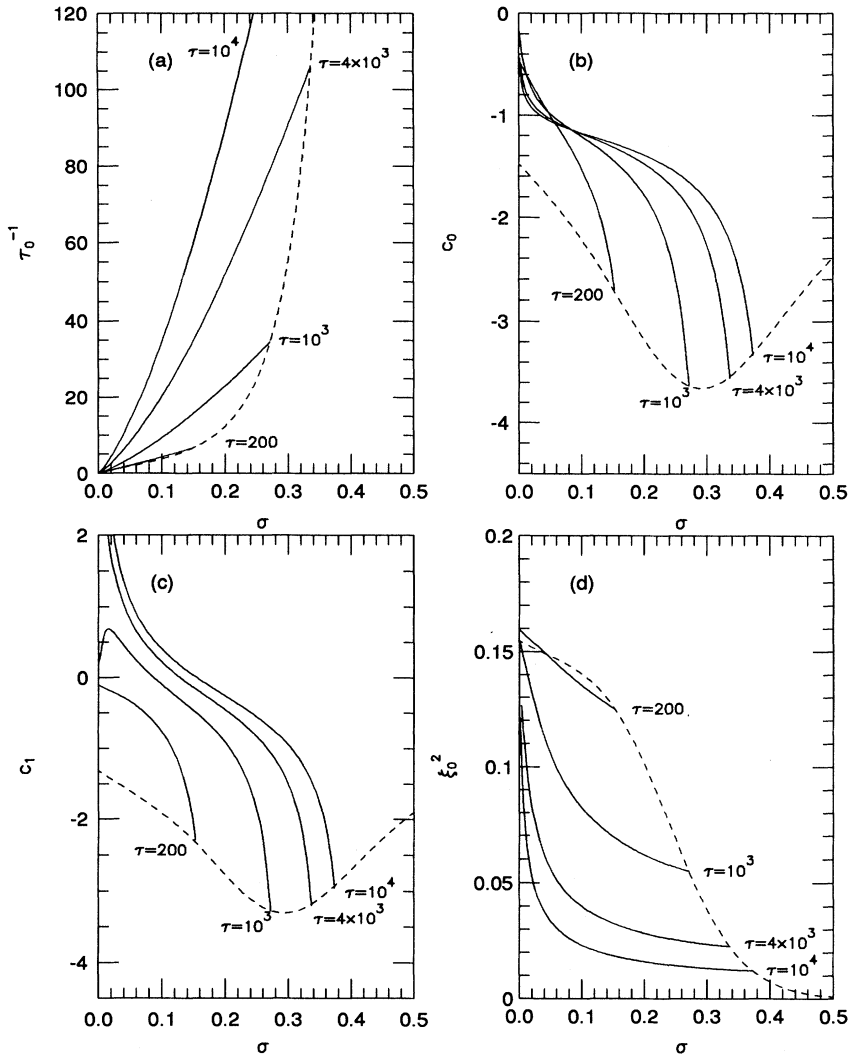

FIG. 9. Same as Fig. 8 but showing the σ dependence for several values of τ.

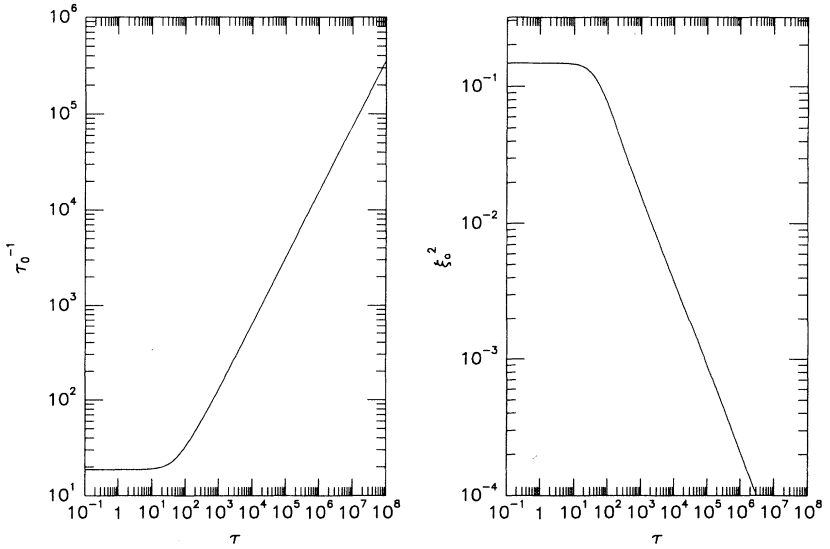

FIG. 10. The coefficients τ_0^{-1} and ξ_0^2 as a function of τ for steady convection for $\sigma = 10$.

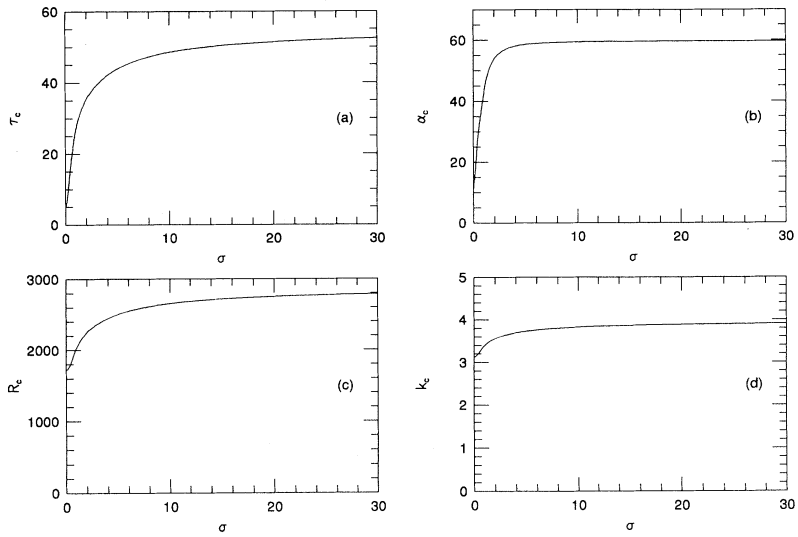

FIG. 11. The onset of the Küppers-Lortz instability as a function of σ. (a) The critical Taylor number τ_c, (b) the critical angle α_c, (c) the corresponding Rayleigh number, and (d) the corresponding wave number.

In the following we use the technique of Sec. III to calculate r_2^{TW} and r_2^{SW}, and use these results to deduce $\mathrm{Re}(a)$ and $\mathrm{Re}(b)$, and hence the stability of each solution type (see Table II). The calculations are carried out for the unconstrained and constrained problems as discussed in Sec. III. In both treatments of the mean flows we find that throughout parameter space, TW and SW bifurcate supercritically. The curve $\mathrm{Re}(b) = 0$ separating stable standing waves from stable traveling waves is found by varying τ for each σ. For the unconstrained case the result is shown as the dashed line in Fig. 3. These results are qualitatively similar to those for the stress-free boundaries [22]: the curve $\mathrm{Re}(b) = 0$ originates on the curve separating stationary and overstable convection with traveling waves preferred above and standing waves preferred below. In contrast to the stress-free case, however, the curve $\mathrm{Re}(b) = 0$ is not monotonic with τ. It starts on the CT curve at very high τ ($\tau = 7 \times 10^5, \sigma = 0.442$), and then decreases, reaching a minimum at $\tau = 1010, \sigma = 0.20$ before increasing again. Notice that the minimum in τ is sufficiently low that it falls within the experimentally realizable parameter range. Note also that in the range $0.442 < \sigma < \sigma^\star = 0.677$ traveling waves are preferred for all $\tau > \tau_{\mathrm{CT}}(\sigma)$. For stress-free boundaries the corresponding range is $0.53 < \sigma < 0.677$. However for the no-slip boundary conditions the corresponding rotation rates are so high that the governing equations [(8a)–(8c)] are unlikely to remain valid. The results for the constrained case are very similar. This is because at high Taylor numbers the mean flows in both the radial and azimuthal directions become very weak; consequently the suppression of the radial mean flow by the sidewalls plays essentially no role at the Taylor numbers for which TW are preferred. For example, at $\sigma = 0.20$, the value corresponding to the minimum of the curve $\mathrm{Re}(b) = 0$ in Fig. 3, the suppression of the radial mean flow increases the value of τ for the transition from SW to TW by two parts in 10^5. Consequently, the presence of the sidewalls manifests itself primarily at the level of the linear stability problem (cf. [10]). In general decreasing the Prandtl number increases the importance of the mean flow [9, 10], but in the present problem this tendency is more than offset by the rapid increase in the minimum Taylor number at which the TW are preferred.

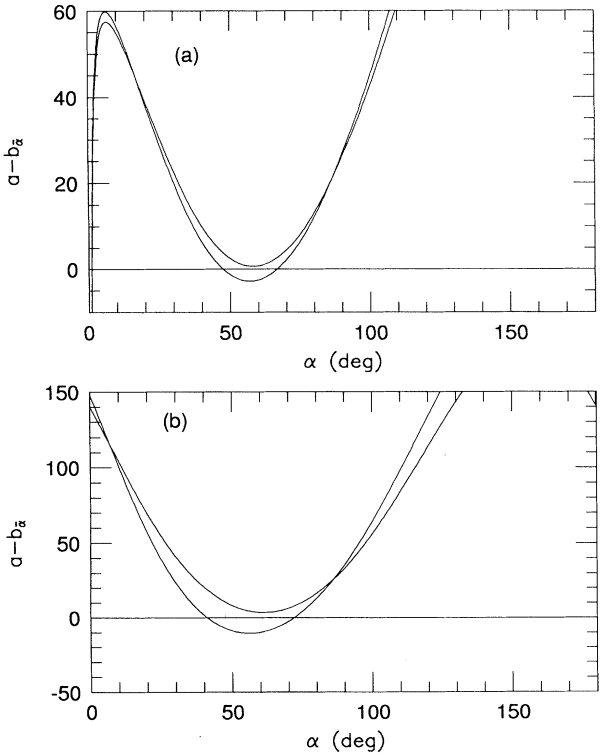

FIG. 12. The quantity $a - b_{\bar{\alpha}}$ for $\sigma = 100$ as a function of α for (a) stress-free boundaries ($\tau = 45, 50$) and (b) no-slip boundaries ($\tau = 50, 65$). For these cases $\tau_c = 46, 54$, respectively. Note that in the stress-free case $a - b_{\bar{\alpha}}$ is always negative for sufficiently small α even when $\tau < \tau_c$.

VII. DISCUSSION

In this paper we have reexamined the linear stability problem and weakly nonlinear theory for both oscillatory and steady convection in a rotating layer. We have focused on providing predictions for recent and ongoing experiments on this system. These experiments use state of the art measurement techniques and have focused on low to moderate Prandtl number fluids ($0.49 \leq \sigma < 1.0$), a range that has hitherto been largely unexplored experimentally. Consequently this range has not been greatly emphasized in earlier theoretical treatments, in spite of the fact that it contains the transition from steady to overstable convection. In addition to computing the critical Rayleigh numbers, wave numbers, and Hopf frequencies for the experimental parameter values and boundary conditions, we have also determined the threshold values of the Taylor number and the corresponding angle for the Küppers-Lortz instability. This instability has been the focus of several of the recent experiments [4,5,17,18]. For the low Prandtl numbers relevant to the latter two experiments substantial departures of τ_c and α_c from their large Prandtl number values have been revealed. However, at the present time any quantitative comparison between the theory and the experiments appears to be plagued by finite-size effects (cf. [4]).

In the overstable regime a two-dimensional calculation has revealed in the experimentally accessible parameter range a preference for standing waves near onset. This result is perhaps not surprising, but suggests that in contrast to traveling waves that are characteristic of binary fluid mixtures, standing waves might become accessible to experiments in large-aspect-ratio rotating convection with sufficiently low Prandtl number. A recent theoretical study of three-dimensional overstable convection [27] indicates that a much larger number of competing spatially periodic patterns becomes available in three dimensions, suggesting the possibility that the standing waves that are stable in two dimensions might actually be unstable to other patterns in three dimensions. This is the case, for example, for compressible convection in a vertical magnetic field [30]. In addition, Ref. [27] discusses in detail the character of possible Küppers-Lortz-like instabilities of the traveling and standing waves described here. Such instabilities may become important with increasing rotation rate, as in the case of steady rolls discussed in Sec. V. They are, however, beyond the scope of the present paper.

It is important to relate the results obtained here to the experiments in a little more detail. In a recent paper Goldstein *et al.* [31] observe that in a rotating cylinder the onset of convection can be either in the form of a wall mode or a body mode, depending both on the rotation rate and the cylinder aspect ratio. The former is a mode confined to the periphery of the cylinder; the latter is a mode that fills the interior of the container but has small amplitude near the wall. The wall modes always have a nonzero azimuthal wave number and hence precess in the rotating frame. Only body modes with a zero azimuthal wave number do not precess. It is these modes that are to be identified directly with the modes discussed in the present paper, a pattern of parallel rolls forming a local approximation to a pattern of concentric rolls. It is for this reason that the traveling waves considered above propagate in the radial direction, and hence always towards a sidewall. The present paper can therefore be viewed as a contribution towards the study of nonlinear oscillatory convection in rotating cylindrical containers. In contrast the effect of the container walls on the Küppers-Lortz instability remains uncertain. The calculations of Goldstein *et al.* also show that the differences in the critical Rayleigh numbers for stress-free and no-slip boundary conditions disappear already for $\tau \approx 400$ even in containers of quite small aspect ratio. However, in this case no asymptotic analysis analogous to that presented in Sec. IV is available. There seems little doubt, however, that the reason for this behavior is identical to that for a plane layer.

ACKNOWLEDGMENTS

This work was supported by the National Science Foundation under Grant No. DMS-8814702 and the Isaac Newton Institute for Mathematical Sciences in Cambridge, United Kingdom.

[1] P. Kolodner, C. M. Surko, and H. Williams, Physica D **37**, 319 (1989).
[2] V. Steinberg, J. Fineberg, E. Moses, and I. Rehberg, Physica D **37**, 359 (1989).
[3] G. Küppers and D. Lortz, J. Fluid Mech. **35**, 609 (1969).
[4] F. Zhong, R. Ecke, and V. Steinberg, Physica D **51**, 596 (1991).
[5] F. Zhong and R. Ecke, Chaos **2**, 163 (1992).
[6] J. D. Crawford and E. Knobloch, Annu. Rev. Fluid Mech. **23**, 341 (1991).
[7] E. Knobloch and M. Silber, in *Nonlinear Structures in Physical Systems–Pattern Formation, Chaos and Waves*, edited by L. Lam and H. C. Morris (Springer-Verlag, New York, 1990).
[8] E. Knobloch, Phys. Rev. A **34**, 1538 (1986).
[9] R. M. Clever and F. H. Busse, J. Fluid Mech. **201**, 507 (1989).
[10] T. Clune and E. Knobloch, Physica D **61**, 106 (1992).
[11] W. S. Edwards, R. P. Tagg, B. S. Dornblaser, and H. L. Swinney, Eur. J. Mech. B Suppl. **10** (2), 205 (1991).
[12] E. Knobloch and D. R. Moore, Phys. Rev. A **37**, 860 (1988).
[13] T. Clune (unpublished).
[14] S. Chandrasekhar, *Hydrodynamic and Hydromagnetic Stability* (Oxford University Press, Oxford, 1961).
[15] R. M. Clever and F. H. Busse, J. Fluid Mech. **94**, 609 (1979).
[16] M. R. Ardron, P. G. J. Lucas, and N. D. Stein, Phys. Fluids A **4**, 664 (1992).
[17] Y. Hu, R. Ecke, and G. Ahlers (unpublished).

[18] J. J. Niemela and R. J. Donnelly, Phys. Rev. Lett. **57**, 2524 (1986).
[19] J. M. Pfotenhauer, J. J. Niemela, and R. J. Donnelly, J. Fluid Mech. **175**, 85 (1987).
[20] H. T. Rossby, J. Fluid Mech. **36**, 309 (1969).
[21] P. P. Niiler and F. E. Bisshopp, J. Fluid Mech. **22**, 753 (1965).
[22] E. Knobloch and M. Silber, Geophys. Astrophys. Fluid Dyn. **51**, 195 (1990).
[23] This terminology differs from that employed in Ref. [12].
[24] M. C. Cross and K. Kim, Phys. Rev. A **37**, 3909 (1988); W. Schöpf and W. Zimmermann, Europhys. Lett. **8**, 41 (1989).
[25] G. Küppers, Phys. Lett. A **32**, 7 (1970).
[26] J. W. Swift (private communication).
[27] E. Knobloch and M. Silber, Physica D **63**, 213 (1993).
[28] P. C. Matthews (private communication).
[29] H. F. Goldstein, E. Knobloch, I. Mercader, and M. Net, J. Fluid Mech. **248**, 583 (1993).